A SELF-RESONANT, MEMS-FABRICATED, AIR-BREATHING ENGINE

Florian Herrault[1], Thomas Crittenden[2], Svyatoslav Yorish[2], Edward Birdsell[1], Ari Glezer[1], and Mark G. Allen[1]
[1]Georgia Institute of Technology, Atlanta, Georgia, USA
[2]Virtual AeroSurface Technologies, Atlanta, Georgia, USA

ABSTRACT

This paper reports the design, fabrication, and characterization of a self-resonant, MEMS-fabricated, air-breathing engine. Commonly known as a valveless pulsejet, this device converts chemical energy from fuel into pulsatile thrust which may be used for propulsion or converted into vibrational mechanical energy suitable for electrical power generation. The engine is fabricated by laser machining of ceramic sheets, followed by lamination and sintering. Using hydrogen fuel, the engine resonates in a frequency range of 0.9-1.6kHz with pressure differentials in the combustion chamber up to 10kPa. When coupled with a Lorentz-force type generator, the system delivers 2.5μW to an external electrical load at a frequency of 1.5kHz.

INTRODUCTION

Due to the increasing demand for small-scale, portable, self-powered systems, chemical-to-electrical converters have been an active research area as potential replacements for existing batteries. Hence, efforts have been partly dedicated to heat-engine-based electrical power generation systems [1]. However, while MEMS-based, high power density, mechanical-to-electrical energy converters have been successfully demonstrated [2, 3], MEMS-based, heat engines for chemical-to-mechanical conversion systems remain elusive. As their dimensions shrink, they become difficult to fabricate and operate. First, it is challenging to reproduce the complexity and three-dimensionality of heat engines at a small scale using microfabrication approaches. Secondly, as the size of these converters decreases, the operating frequency required to maintain appreciable output power increases, which in turn results in very high required rotational speeds. Air-driven, silicon-based, multi-wafer, micro-turbines have demonstrated rotational speeds beyond one million of revolutions per minute [1]. In addition, and as a part of the same research effort, micro-combustors have been successfully fabricated [4]. However, severe constraints on materials and fabrication tolerances have been observed. As a result, the fabrication and operation of devices combining the combustor and the turbine for chemical-to-mechanical conversion is still very challenging. Thus, at smaller scales, a tradeoff between simplicity of operation (e.g., no valves, rotating parts, or seals) and ultimate efficiency may be desirable. As a consequence, we investigate the application of MEMS fabrication techniques to the development of a valveless pulsejet, a small-scale, reduced-complexity, air-breathing engine.

Valveless pulsejet combustor designs with no moving parts at larger scales have been known since the early 1900s. Recently, a 15-cm long, conventionally fabricated system has been reported [5, 6], where various system measurements such as temperature, pressure, operation frequency and thrust measurements have been described. To our knowledge, there is no literature reporting on the design, and fabrication of such engines at smaller scales (i.e. combustion chamber volume below 1cm^3). The relatively low efficiency of this type of engine has always been seen as a major drawback as compared to that of other heat engines. However, at a small-scale, this issue is counterbalanced by the extreme simplicity of design and operation, as mentioned previously. In this paper, we present the development of a MEMS-fabricated, ceramic-based, valveless pulsejet supplied by hydrogen. The device converts chemical energy from a source of hydrogen fuel into an oscillating thrust, which can be either used for micro-propulsion, or converted into vibrational mechanical energy. Such energy could be used as a platform for mechanical-to-electrical converters using vibration-based, electromagnetic power generation systems. The air-breathing engine self-resonates in the kHz range; this high mechanical frequency is potentially suitable for high energy density generators.

SYSTEM DESIGN

The self-resonant, air-breathing engine includes a combustion chamber with air and fuel inlets, and a resonant tailpipe. Openings are also designed in the combustion chamber to integrate two spark plugs for initial ignition. Fig. 1 shows a three-dimensional (3-D) rendering of the MEMS-fabricated engine with integrated fuel inlets. As opposed to other heat engines, this combustor does not have any moving parts.

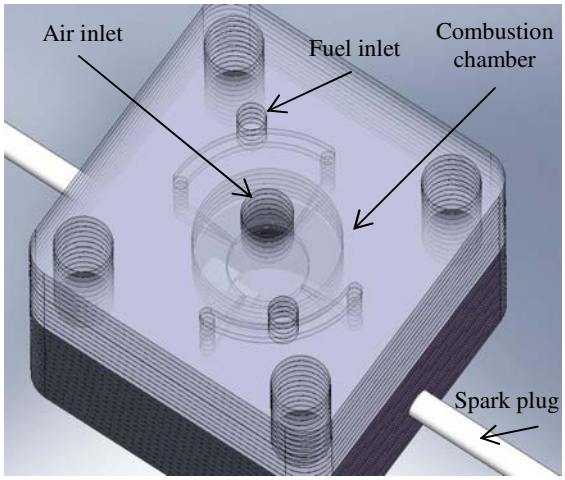

Figure 1: 3-D renderings of the MEMS-fabricated, self-resonant, air-breathing engine with integrated fuel inlets.

Operation Cycle

The typical operation cycle of the air-breathing, self-resonant engine is shown in Fig. 2. As illustrated in Fig. 2a, the cycle begins with a single spark ignition accompanying a small amount of force-fed air into the inlet, and the fuel supply. The spark ignites the fuel/air mixture in the combustion chamber with a corresponding pressure rise, pushing exhaust products out of the inlet pipe and out toward the end of the exhaust pipe, as presented in Fig. 2(b-c). After a short period of time, the pressure in the chamber decays to below atmospheric level, creating a phenomenon of suction. This induces fresh air to flow into the chamber from the air inlet, and hot gases and radicals to return to the chamber from the exhaust pipe, as described in Fig. 2d. Consequently, the combustion is automatically re-ignited without any additional spark, and the sequence (2.b-2.e) resumes as long as fuel is supplied. The net result is an air-breathing engine capable of producing oscillating thrust with no moving parts. Furthermore, the single spark ignition is a major advantage over other combustion engines.

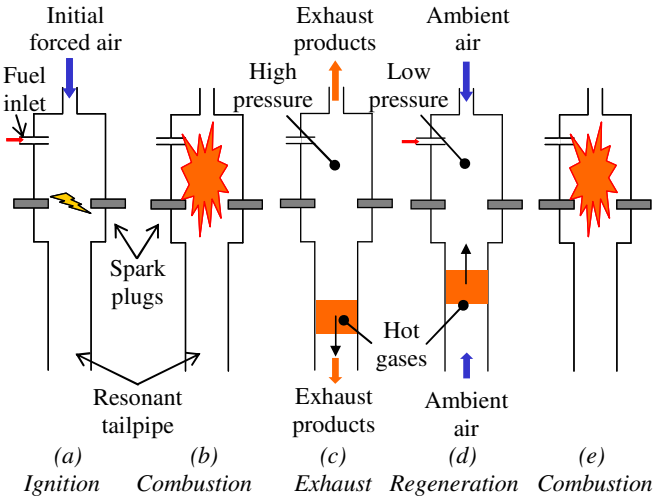

Figure 2: Conceptual schematic of typical valveless pulsejet operation.

SYSTEM FABRICATION

Laser micromachining of ceramic sheets (Alumina A-16), followed by mass-manufacturable lamination and sintering is used to fabricate the primary elements of this device [7, 8]. The three-dimensional design of the device is divided into CAD layers of a thickness of approximately 1mm. Those individual layers are patterned onto ceramic sheets by infrared laser micromachining. The multiple layers are then accurately positioned on top of each other using alignment pins, and laminated for 5min at a temperature of 85°C, and a pressure of 50kg/cm^2. The device is finally sintered at a temperature of 1500°C for several hours. Fig. 3 illustrates the described fabrication concept. Shrinkage of approximately 15% occurs during the sintering process, and must be considered in the design. Such a process enables the integration of complex, three-dimensional microfluidic ports for the fuel and air inlets, the exhaust as well as the spark initiation.

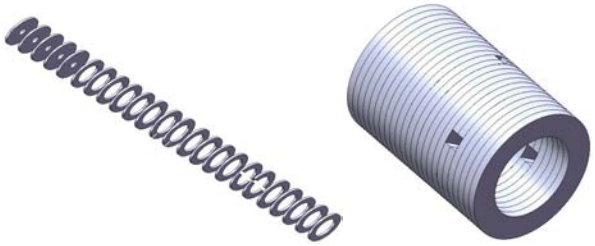

(a) (b)

Figure 3: Conceptual renderings of laser micromachined, laminated sheets: (a) Ceramic layers are individually laser machined, (b) and then aligned, laminated, and finally sintered.

First generation air-breathing engine

The first generation device has been fabricated by stacking laser machined rings with integrated ports, as illustrated in Fig. 4. The fabricated elements of the first generation device are shown in Fig. 5. The combustion chamber has an inner diameter of 7.5mm, and an internal volume of approximately 0.8cm^3. As shown in Fig. 5c, the experimental setup consists of the hydrogen feed line, and the conventional, 3.2mm diameter, resonant tailpipe. The area ratios between the air inlet, combustion chamber, and resonant tailpipe are critical for the operation of the engine. If the amount of air that is sucked back in the chamber is too low, the device will not resonate. In addition, if the exhaust pipe is too short, the hot gases will not remain within it, which will prevent the regeneration phase from taking place. Operating conditions have been determined by experimental investigations.

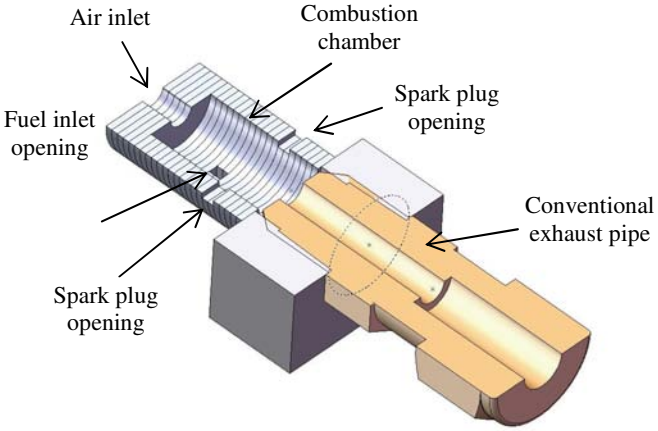

Figure 4: 3-D cross-sectional renderings of the self-resonant combustion device with conventional exhaust pipe.

Note that the inlet system and the combustion chamber have been fabricated separately to allow testing of several inlet and exhaust configurations with the same chamber.

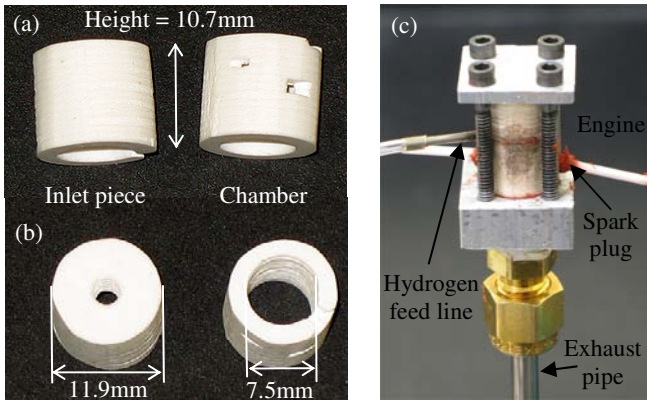

Figure 5: Self-resonant, combustion engine: The air inlet piece has been fabricated separately to test different configurations with the same combustion chamber: (a) Side-view, (b) Top-view, and (c) Test setup.

Second generation air-breathing engine with integrated inlets

Proper designs of the fuel and air inlets are required to obtain the correct gas mixture, and an operating device. Large-scale devices integrate conventional pipes to supply the fuel inside the chamber [5, 6]. MEMS fabrication approaches offer the opportunity of fully integrated, microfluidic inlet channels. In addition, complicated, and non-conventional designs can be achieved. Fig. 6 depicts the second generation device with integrated, multi-directional fuel inlets. The four inlets are located at the periphery of the chamber, and direct the flow of fuel toward the center of the chamber. The combustion chamber, which is shown in Fig. 6c, is similar to the first generation engine, and the same resonant tailpipe has been used for system characterization.

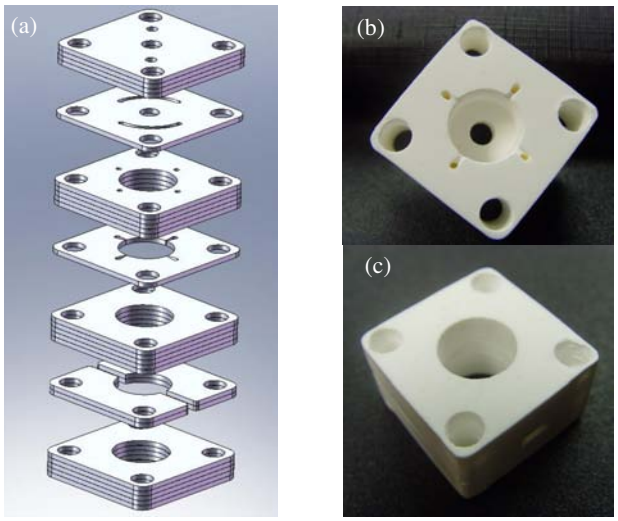

Figure 6: Self-resonant, air-breathing engine with integrated fuel inlets: (a) Exploded rendering of the design, (b) Integrated, multi-directional fuel/air inlet, and (c) Combustion chamber.

SYSTEM CHARACTERIZATION

First generation device

A pressure transducer is implemented to measure the variation of pressure inside the combustion chamber as a function of time and fuel flow-rates. The acquisition of the data is performed with the assistance of LabView software. A 1mm diameter opening that is located in the center of the combustion chamber is integrated in the fabrication process to allow the pressure measurements. Fig. 7 depicts the time-dependent pressure variation. At a hydrogen flow rate of 2.5L/min, a pressure differential of 9kPa, and a resonant frequency of 1.38kHz have been measured. The pressure differential is calculated by measuring the peak-to-peak values between the high pressure and the low pressure phases. As can be seen, the pressure goes below the atmosphere level as previously detailed in the operation cycle in Fig. 2.

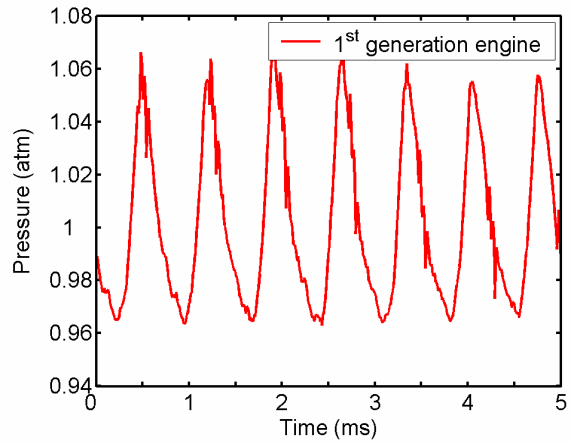

Figure 7: First generation device: Pressure variation as a function of time using a hydrogen flow-rate of 2.5L/min.

As shown in Fig. 8, both the resonant frequency and the pressure differential vary with hydrogen flow rates. Furthermore, the fabricated combustion engine resonates for flow rates in the 1-4L/min range where the air/fuel mixing occurs properly. A maximum of 10kPa of pressure differential has been measured inside the chamber.

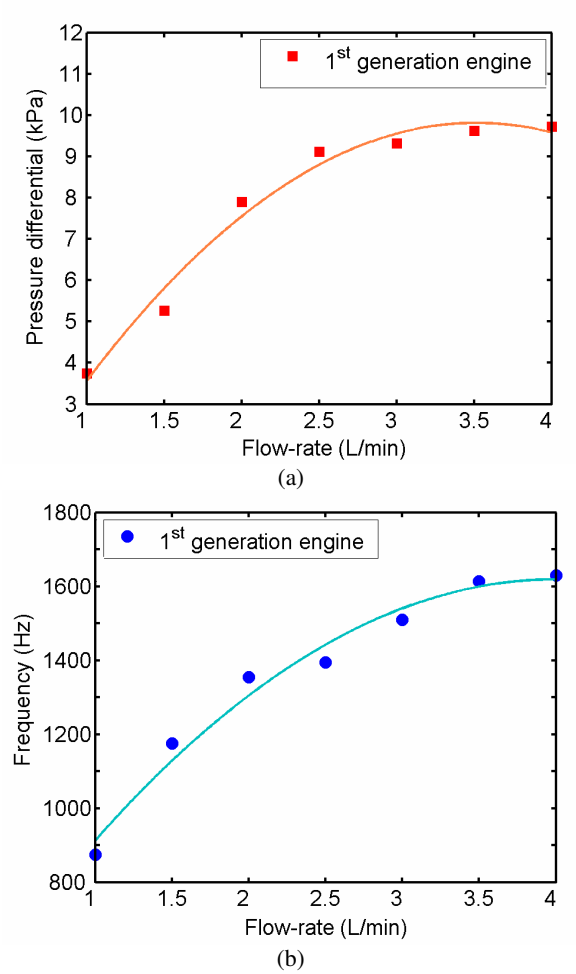

Figure 8: First generation device: (a) Pressure differential and (b) resonant frequency as a function of hydrogen flow-rate.

The flow structure of the air inlet has been recorded using a Schlieren system. Schlieren flow visualization is an optical system based on the deflection of light. Because the jet is three-dimensional, and there is significant wasted heat, it is difficult to have a clear picture of the phenomenon. The suction phase, or regeneration phase, is shown in Fig. 9.

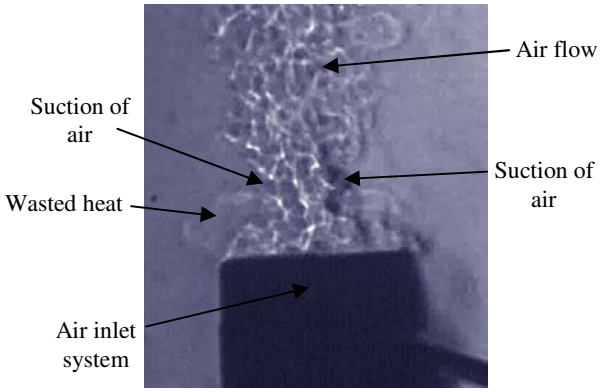

Figure 9: Visualization of the air flow on the inlet side using a Schlieren optical system.

Second generation device

Similar experiments have been performed using the engine with integrated, multi-directional fuel inlets. The pressure variation as a function of time is shown in Fig. 10 for a hydrogen flow-rate of 2L/min. The functional range of operation has been measured from approximately 1L/min to 3L/min. However, both the resonant frequency and the pressure differential vary with time, as depicted in Fig. 10. This is presumably due to unequal mixing and also ineffective mixture ratio from pulse to pulse in this unoptimized structure. In this regard, having the fuel inlet at the center of the chamber yields better results than having the fuel inlets on the periphery. Since the primary air flow is along the centerline of the chamber, the hydrogen needs to penetrate to the center of the chamber and have enough time to remain for complete mixing on the time scale of the resonator.

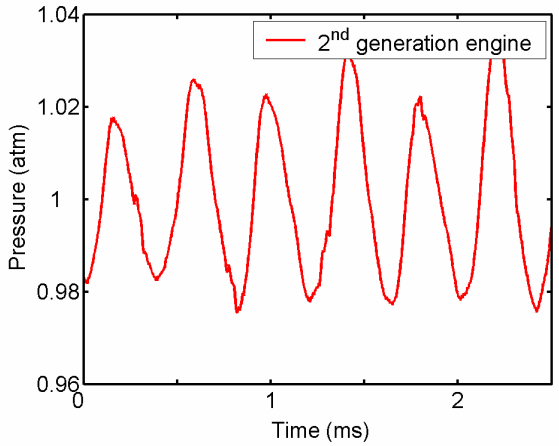

Figure 10: Second generation device: Pressure variation as a function of time using a hydrogen flow-rate of 2L/min.

Electrical Power Measurements

To demonstrate the feasibility of electrical power generation using the air-breathing engine as a source of mechanical energy, an electromagnetic, Lorentz-force type generator has been placed in fluidic contact with the engine exhaust. The generator membrane is mechanically driven by the oscillating thrust of the device. As a result, electrical power is delivered to an external load resistance. The first version of the air-breathing engine has been used for this experiment. The results are presented in Fig. 11. An output voltage of approximately $40mV_{rms}$ peak to peak has been measured across an 8Ω load at a frequency of 1.5kHz, which corresponds to an output power of $2.5\mu W_{rms}$. Although this experiment is not optimized for maximum efficiency and high power output, it demonstrates the potential for MEMS-scale, combustion-based fuel-to-electrical power generation. More robust mechanical power transmission is expected to produce significantly higher electrical output.

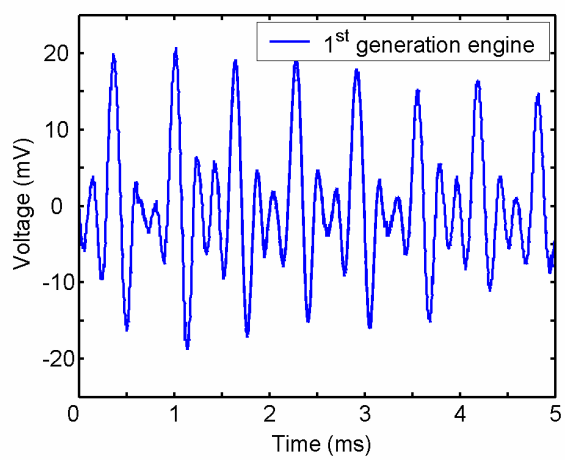

Figure 11: First generation device: Electrical output as a function of time measured by placing a Lorentz-force generator in fluidic contact with the oscillating exhaust. (Hydrogen flow-rate = 3.5L/min).

CONCLUSIONS

We have introduced the fabrication and measurement results of a small-scale, self-resonant, ceramic-based, air breathing engine. When supplied by hydrogen fuel, the system generates a pressure differential up to 10kPa inside the combustion chamber, at a resonant frequency of 1.5kHz. Improvements may include the use of hydrocarbon fuels, or higher level of compactness of the engine. Furthermore, the implementation of a vibration-based magnetic power generator onto the self-resonant engine is envisioned as the next step toward a fully-integrated, MEMS-based, chemical-to-electrical converter, as suggested by the last detailed experiment.

REFERENCES

[1] Epstein, *et al.*, "Power MEMS and Microengines", *Proc. Transducers '97*, pp. 753-756, vol. 2, (1997).

[2] D. P. Arnold, F. Herrault, I. Zana, J.-W. Park, S. Das, J. H. Lang, and M. G. Allen, "Design optimization of an 8 W, microscale axial-flux, permanent-magnet generator," *J. Micromech. Microeng.,* v. 16, n. 9, pp. 290-296, (2006).

[3] H. Raisigel, O. Cugat, and J. Delamare, "Permanent magnet planar micro-generators," *Sensors and Actuators A,* vol. 130-131, pp. 438-444, (2006).

[4] C. M. Spadaccini, A. Mehra, J. Lee, X. Zhang, S. Lukachko, and I. A. Waitz, "High power density Silicon combustion systems for micro gas turbine engines," *J. Eng. Gas Turbines Power,* vol. 125, issue 3, pp. 709–719, (2003).

[5] T. Geng, M. A. Schoen, A. V. Kuznesov, and W. L. Roberts, "Combined numerical and experimental investigation of a 15-cm valveless pulsejet," *Flow turbul. Combust.*, vol. 78, n. 1, pp. 17-33, (2007).

[6] Schoen, M.: "*Experimental investigations in 15 centimeter class pulsejet engines*," Master dissertation, Mechanical and Aerospace Engineering Department, North Carolina State University, Raleigh, North Carolina, (2005).

[7] M. G. Allen, and A. Glezer, "Alternative Micromachining Technologies for the Realization of Robust MEMS," *American Institute of Aeronautics and Astronautics Conference*, AIAA 2000-248, (2000).

[8] E. Birdsell, J. Park, and M. G. Allen, "Wireless ceramic sensors operating in high temperature environments," *40th AIAA Joint Propulsion Conference*, AIAA 2004-3990, (2004).